

# Simulation of drift capacity for RC walls with different section configurations

Susumu Kono, Taku Obara, Rafik Taleb and Hidekazu Watanabe

*Tokyo Institute of Technology, Yokohama, Japan*

Masanori Tani

*Kyoto University, Kyoto, Japan*

Masanobu Sakashita

*Building Research Institute, Tsukuba, Japan*

**ABSTRACT:** A series of experimental studies were conducted on reinforced concrete walls last several years in Japan in order to study compression controlled flexural failure which was observed in the 2010 Chile earthquake and the 2011 Christchurch earthquake. This paper numerically simulates the ultimate drift capacities of RC walls by using twenty-four reinforced concrete wall specimens from these experimental studies. A simple fiber based analysis combined with Beyer's shear drift model is able to provide loads and drifts of ultimate points by choosing a proper set of equivalent plastic hinge length ( $l_p$ ) and the limit strain of confining reinforcement ( $\varepsilon_m$ ). This study shows that various combinations of  $l_p$  and  $\varepsilon_m$  provide good results with similar errors.

## 1 INTRODUCTION

Many RC walls suffered compression controlled flexural failures due to crushing of concrete or buckling and fracture of longitudinal reinforcement at boundary regions in the 2010 Chile Off-Maule Earthquake and 2011 Christchurch Earthquake (AIJ 2012). Based on damage observations in two earthquakes, the engineering society strongly felt that it is necessary to evaluate the ultimate drift capacity and failure mode of RC walls with higher accuracy.

Twenty-four RC wall specimens (Kono et al. 2014, Kabeyasawa et al. 2014, Takahashi et al. 2013, Ogura et al. 2014) were chosen to study their ultimate drift capacities using a simple fiber based analysis. Fiber based analyses have been frequently conducted by many researchers (for example Pugh et al. 2014) to provide a simple design tool for practicing engineers. One of the advantages of fiber based analyses is the simplicity and stability although it is not very easy to properly determine equivalent plastic hinge length and no-flexural drift components such as shear and pull-out drift components (Aaleti et al. 2014, Beyer et al. 2011). Some advanced codes consider the shear - flexure interaction (Martinelli 2011) or even shear - flexure - axial interaction (Mostafaei and Kabeyasawa 2008).

This study compares simulated ultimate drift capacities to experimental results to validate a fiber based analysis for better understanding the seismic performance and preventing collapse of reinforced concrete walls.

## 2 EXPERIMENTAL PROGRAM

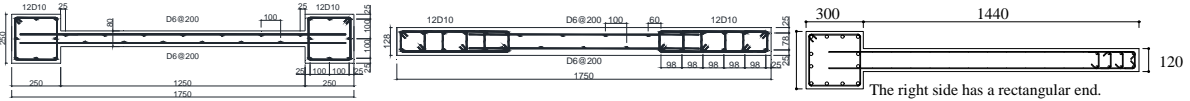
Twenty-four specimens in Table 1 were used in the numerical study since the authors have full or partial access to dimensions, fabrication procedures, and the loading data.

- Flexural yielding was designed to proceed flexural or shear failure for all specimens except #15 (NSW2). NSW2 failed in shear before reaching flexural yielding but other specimens had flexural yielding followed by ultimate flexure or shear failure. Observed failure modes are listed in the table.
- Five specimens from #20 through #24 were asymmetric (AS.) and the other specimens were symmetric. Three representative sections are listed in Figure 1. They are a symmetric barbell section and a symmetric rectangular section with boundary regions (Kono et al. 2014). Figure 1(c) shows that the right edge of an asymmetric section had tie confinement (Takahashi et al. 2013).

Table 1: Major properties and variables of wall specimens.

No.	Specimen	Ref. *1	Observed failure mode *2	Section configuration *3	Elevation size $L_w \times H$ (mm) *4	Confined area *5			Wall panel *6			Cylinder compressive strength (MPa) *7	Axial load level *8	Shear span ratio *9			
						size (mm)	Vert. rebar	Volume ratio of confining rebars	Vert. rebar	Hor. rebar	Thickness (mm)						
1	BC	Kono et al. 2014	F	Barbell	1500x1700	200x200	8-D10	1.20%	2-D4@80	91	35.2	0.047	1.60				
2	NC		Rec.	120x200		1.96%		80						59.5	0.112		
3	BC40		F	Barbell	1750 x 2800	250x250	8-D10		2.26%	D6@100 staggered	128	27.5	0.104			1.71	
4	BC80		F			128x520		12-D10	4.23%								
5	NC40		F	Rec.	1750 x 1700	84x214	10-D10	1.35%	2-D4@50	120	29.6	0.206	1.37				
6	NC80		F			84x114		6-D10						1.45%			
7	MC		F			10-D10		2.59%									
8	SC		F	Barbell	1650x1250	250x150	10-D10	1.58%	2-D4@80	100	32.1	0.075	1.40				
9	HN		F			1750 x 1250		150x250						1.45%			
10	WA1D	F	Rec.			1250		150x300						8-D13	1.31%	2-D4@50	150
11	WB1D	F	100x450	12-D10	1.93%	2-D4@75	100	31.2	0.124								
12	WC1D	F+S	Ogura et al. 2014	Rec.	1050 x 2100	No confined region	2-D13	No shear rebars	2-D10@250	120	24.2	0.150	1.00				
13	WD1D	F+S												120x206	4-D13	2.50%	1-D10@250
14	NSW1	F												200x250	2-D10@200	1.40%	
15	NSW2	S												240x300		12-D10	0.65%
16	NSW3	F												110x220	8-D10	1.71%	2-D10@100
17	NSW4	F												900x1800	200x250	1.40%	2-D10@35
18	NSW5	F	Takanashi et al. 2013	AS. Barbell	1740 x 1200	110x393	10-D10	2-D4@100	120	45.5	0.039	1.45					
19	NSW6	F											240x300	12-D10	0.65%	2-D4@35	
20	C	F											110x220	8-D10	1.71%	2-D4@35	
21	NM3	F											110x393	10-D10	1.90%	2-D4@70	
22	N	F	110x393	10-D10	5.63%	3.81%	2-D4@100	120	45.5	0.054	3.13						
23	N(s70)	F										1.90%	42.6				
24	N(MQd3.1)	F								38.9	0.053						

\*1: References are listed. \*2: Observed failure modes are listed. F: flexural failure. S: Shear failure. F+S: Shear failure after flexural yielding. \*3: "Rec." represents rectangular section. "AS." represents asymmetric section, otherwise sections are symmetric. Five specimens from #15 through #18 are listed as "AS Barbell" or "AS Rec." by looking at the weaker side. \*4:  $L_w$  and  $H$  denotes external wall length and height of wall panel, respectively. \*5: Volume ratio of confining reinforcement is computed for core concrete. The size of core concrete is defined by center to center distance of confining reinforcement. \*6: NSW1, 2, 3 and 4 are lightly reinforced walls without confined end region. \*7: Values are based on cylinder compression tests. \*8: Values are computed based on the gross area of columns and a wall panel. \*9: Height of contraflexure point is divided by  $L_w$  (external wall length).



(a) Symmetric barbell section (b) Symmetric rectangular section (c) Asymmetric section  
Figure 1: Plan view of three representative specimens (Unit: mm).

### 3 NUMERICAL SIMULATIONS OF TEST RESULTS

#### 3.1 Basic concept of modelling

The ultimate drift ratio ( $R_u$ ) is computed by summing the flexural drift component,  $R_{uf}$ , and the shear drift component,  $R_{us}$ , as Eq. (1).

$$R_u = R_{uf} + R_{us} \quad (1)$$

Although, a drift component due to pullout from the stub is not negligible, it is not modelled explicitly but included in  $R_{uf}$  for simplicity.

#### 3.2 Ultimate flexural drift, $R_{uf}$

The flexural drift component,  $R_{uf}$ , is assumed to consist of elastic component,  $R_y$ , and plastic component,  $R_{ufp}$ , as shown in Figure 2(a). Two components are computed based on the idealized curvature distribution in Figure 2(b) and their summation makes  $R_{uf}$  as Eq. (2).

$$R_{uf} = R_y + R_{ufp} = \frac{1}{H} (\Delta_y + \Delta_{ufp}) \quad (2)$$

$$\Delta_{ufp} = l_p \phi_{ufp} (H - 0.5l_p) \quad (3)$$

$$\Delta_y = \frac{Q_u H^3}{3EI} \quad (4)$$

where elastic drift ratio,  $R_y = \Delta_y/H$ , is computed from a linear elastic curvature distribution over the height. The plastic drift ratio,  $R_{ufp} = \Delta_{ufp}/H$ , is computed from a uniform plastic curvature,  $\phi_{ufp}$ , over the equivalent plastic hinge height,  $l_p$ . Then,  $\Delta_{ufp}$  is the ultimate plastic drift displacement,  $\Delta_y$  is the elastic drift displacement when the plastic drift reaches  $\Delta_{ufp}$ ,  $\phi_{ufp}$  is the ultimate plastic curvature over the plastic hinge,  $Q_u$  is the shear force when  $\phi_{ufp}$  is reached, and  $EI$  is the flexural stiffness of the wall.

A fiber based analysis is carried out to compute plastic flexural drift component,  $\Delta_{ufp}$ . Different fibers represent elements for either plain concrete, confined concrete and vertical reinforcing bars. Plain concrete of wall panels and covers is modelled with Popovics model (1973) (Figure 3(a)). The peak point of stress-strain relation for confined concrete is simulated by Sakino - Sun model (1994) and Popovics model was again used to describe its stress-strain relation (Figure 3(a)). The stress-strain relations for vertical reinforcing bars were modelled with tri-linear curves (Figure 3(b)). Once a set of shear force,  $Q_u$ , and plastic drift component,  $R_{ufp}$ , is obtained, corresponding  $R_y$  can be computed using a basic elastic theory as  $\Delta_y = Q_u H^3 / (3EI)$ .

$R_f$  is considered to reach  $R_{uf}$  when one of following three conditions is met. In the numerical simulation for twenty-four specimens, #1 did not happen and #2 governed most of the specimens.

1. When the load carrying capacity decreases to 80% of the peak load.
2. When the extreme compressive fiber strain of core concrete reaches the ultimate limit strain,  $\epsilon_{cu}$ . This study uses Mander's model expressed by Eq. (6).
3. When the strain of tensile vertical reinforcing bars reaches the ultimate limit strain. This study uses 0.15.

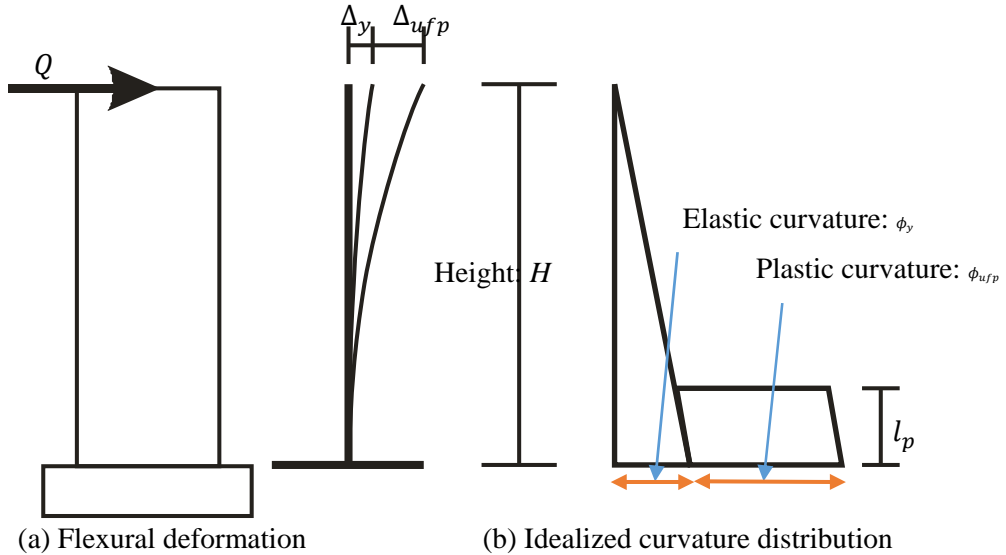
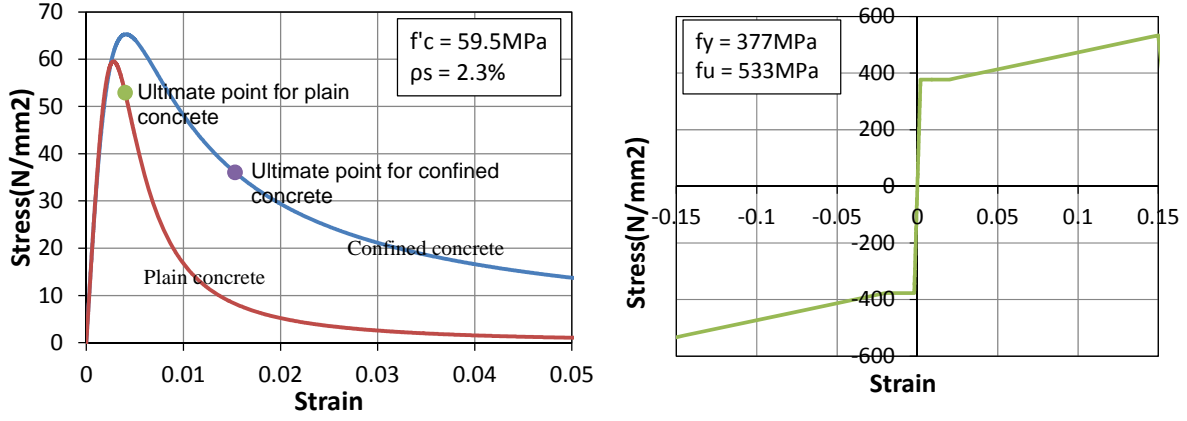


Figure 2: Decomposition of ultimate flexural drift component



(a) Plain and confined concrete (b) Steel reinforcement  
Figure 3: Numerical model of stress –strain relations for BC40

The ultimate limit strain of confined concrete,  $\varepsilon_{cu}$ , is computed with Mander's model (Mander et al. 1988, Paulay and Priestley 1992) as Eq. (5).

$$\varepsilon_{cu} = 0.004 + 1.4\rho_s f_{yh} \varepsilon_m / f'_{cc} \quad (5)$$

where  $f'_{cc}$  is the compressive strength of confined concrete computed using Sakino-Sun model,  $\varepsilon_m$  is the steel strain of confining reinforcement at the maximum tensile stress,  $\rho_s$  and  $f_{yh}$  is the volumetric ratio and yield strength of confining reinforcement, respectively. In this study,  $\varepsilon_m$  is considered as the limit strain of confining reinforcement and its rational value was studied. The ultimate point of concrete for BC40 is marked in Figure 3(a) as an example.

### 3.3 Ultimate shear drift, $R_{us}$

Beyer et al.'s model (2011) is used to simulate the shear drift component. This model allows the estimation of the ratio of shear-to-flexural deformations for shear walls whose shear-transfer mechanism is not significantly deteriorating. The ratio of shear drift,  $R_{us}$ , to flexural drift,  $R_{uf}$ , is expressed as Eqs. (6) and (7).

$$\frac{R_{us}}{R_{uf}} = 1.5 \frac{\varepsilon_{mean}}{\phi H \tan \beta} \quad (6)$$

$$\beta = \tan^{-1} \left\{ \left( \frac{jd}{v} \right) \left( f_l b_w + \frac{A_{sw} f_{yw}}{s} \right) \right\} \leq 90^\circ \quad (7)$$

where  $\varepsilon_{mean}$  is the axial strain at the center of gravity of the wall section,  $\phi$  is the curvature at the critical section,  $H$  is the shear span. Variable  $\beta$  is the cracking angle measured against the element axis and assumed 45 degrees in this study, which is suggested by Beyer et al. for simplification. Variables  $\varepsilon_{mean}$  and  $\phi$  are known values from the fiber based analysis. With this equation, the shear drift component can be obtained with an easy and stable manner once the flexural drift component is computed.

### 3.4 Simulation procedures

Six equations for equivalent plastic hinge length,  $l_p$ , is listed in Table 2. Index  $\alpha$  in #1 is taken as 0.2, 0.33, and 0.5 and Index  $\beta$  in #2 was taken as 4. After all, eight patterns were tested for plastic hinge length and the equivalent plastic hinge length roughly ranges from 200mm to 1000mm for twenty-four specimens.

The limit strain of confining reinforcement,  $\varepsilon_m$ , in Eq. (5) is taken between 1% and 8% at one percent increment (eight types). By combining eight  $l_p$ 's and eight  $\varepsilon_m$ 's, over 50 combinations for  $l_p$  and  $\varepsilon_m$  were computed for each specimen to search the best combination to simulate ultimate drift.

Table 2: Existing equations to compute equivalent plastic hinge length.

No.	Reference	Equation
1	Kono et al. (2014) Kowalski (2011) Thomsen and Wallace (2004)	$l_p = \alpha l_w$ ( $\alpha$ was taken as 0.2, 0.33 and 0.5.)
2	Takahashi et al. (2013) Kabeyasawa et al. (2011) Wallace and Moehle (1992)	$l_p = \beta t_w$ ( $\beta$ was taken as 4.)
3	Paulay and Priestley (1992)	$l_p = 0.2l_w + 0.044H$
4	Priestley et al. (1996)	$l_p = 0.08H + 0.15f_y d_b l_w$
5	Panagioraks and Fardis (2001)	$l_p = 0.12H + 0.014f_y d_b l_w$
6	Bohl and Adebar (2011)	$l_p = (0.2l_w + 0.05H)(1 - 1.5 P / (f'_c A_g)) < 0.8l_w$

$H$  = shear span,  $l_w$  = length of wall,  $d_b$  and  $f_y$  = diameter and yield strength of longitudinal reinforcement, respectively.  $P$  = axial load,  $f'_c$  = concrete compressive strength,  $A_g$  = wall cross-section area

### 3.5 Simulation results

A set of  $l_p$  and  $\varepsilon_m$  were optimized to best simulate the ultimate drifts of fourteen specimens (#1 through #13, and #23), which were symmetric and had confined end regions. The concept of the ultimate limit strain by Mander et al. relatively well functions for these specimens due to confined end region. Simulations are conducted for each case of equivalent plastic hinge length and the best  $\varepsilon_m$  for each  $l_p$  is shown in Table 3, which also shows mean and standard deviation of  $R_{u-exp}/R_{u-cal}$ . Panagioraks and Fardis's model has slightly higher standard deviation but other models give similarly acceptable results. Among them, three cases were chosen for further discussion since they show a wide variation of  $l_p$ .

1.  $l_p = 0.2l_w$  and  $\varepsilon_m = 6\%$ . (mean=1.07, stv=0.19)
2.  $l_p = 0.33l_w$  and  $\varepsilon_m = 2\%$ . (mean=0.98, stv=0.17)
3.  $l_p = 0.5l_w$  and  $\varepsilon_m = 1\%$ . (mean=0.90, stv=0.17)

Table 4 shows statistics of these three cases for the ultimate drift capacity and its load. The results for  $R_{u-exp}/R_{u-cal}$  are not good for ten remaining specimens. On the other hand, the results on load ( $Q_{u-exp}/Q_{u-cal}$ ) are similarly acceptable for three cases on both fourteen selected and ten remaining specimens.

In order to study the scatter of data shown in Table 4, the experimental and simulated drifts are shown in Figure 4 for fourteen selected and ten remaining specimens, respectively, for Case 2 ( $l_p = 0.33l_w$  and  $\varepsilon_m = 2\%$ ). In Figure 4(b), large errors occur for specimens with large shear sliding and specimens with no confined regions. NSW6 had large drift capacity in the experiment and its value is much higher than the prediction.

Table 4 shows that Case 1, Case2 and Case 3 are similarly good. Equivalent plastic hinge length for Case 1 and Case 3 are nearly the minimum and maximum extremes for eight cases and Case 2 ( $l_p = 0.33l_w$  and  $\varepsilon_m = 2\%$ ) takes the intermediate values. This demonstrates that various combinations of  $l_p$  and  $\varepsilon_m$  make equally good agreement with experimental drift capacity.

The effects of cyclic loading is neglected since the analysis is monotonic. The cyclic effects are important to rigorously simulate the wall under seismic loading. If the flexural failure is controlled by buckling of vertical reinforcement (Dodd and Restrepo 1995), a simple monotonic simulation may not be able to catch the point of ultimate failure point due to bar buckling. This aspect is left to the future study.

Table 3: Statistics of selected simulation results for 14 selected specimens.

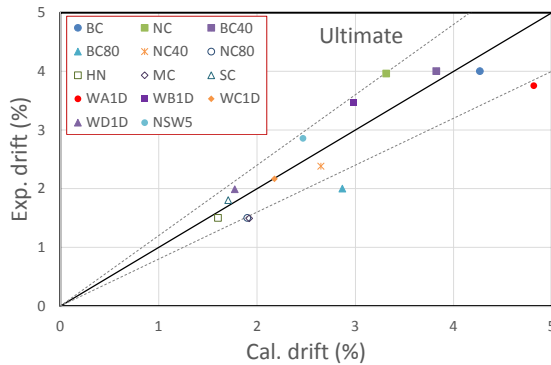
No.	Equation for $l_p$	$\varepsilon_m$ *1	$R_{u-exp}/R_{u-cal}$	
			mean	std
1-1	$l_p = 0.2l_w$	6%	1.07	0.19
1-2	$l_p = 0.33l_w$	2%	0.98	0.17
1-3	$l_p = 0.5l_w$	1%	0.90	0.17
2	$l_p = 4t_w$	4%	0.96	0.20
3	Paulay and Priestley (1992)	4%	0.98	0.18
4	Priestley et al. (1996)	1%	1.02	0.22
5	Panagioraks and Fardis (2001)	8%	1.26	0.42
6	Bohl and Adebar (2011)	4%	0.98	0.18

\*1:  $\varepsilon_m$  was chosen for the best results for given  $l_p$ .

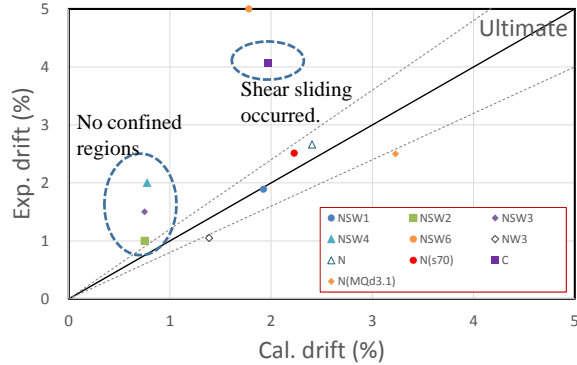
Table 4: Ratio of experimental to computed results in terms of drift ( $R_{u-exp}/R_{u-cal}$ ) and load ( $Q_{u-exp}/Q_{u-cal}$ ).

Item	*1 $l_p$ and $\varepsilon_m$	Type	$R_{u-exp}/R_{u-cal}$		$Q_{u-exp}/Q_{u-cal}$	
			14 selected specimens	10 remaining specimens	14 selected specimens	10 remaining specimens
Ru-exp/Ru-cal	$l_p=0.2l_w, \varepsilon_m=6\%$	mean	1.07	2.54	0.93	0.85
		std	0.19	1.49	0.10	0.08
	$l_p=0.33l_w, \varepsilon_m=2\%$	mean	0.98	1.84	0.89	0.84
		std	0.17	0.99	0.05	0.06
	$l_p=0.5l_w, \varepsilon_m=1\%$	mean	0.90	1.48	0.89	0.83
		std	0.17	0.77	0.04	0.06

\*1: Equivalent plastic hinge length ( $l_p$ ), and the limit strain of confined reinforcement ( $\varepsilon_m$ ) are listed. \*2: Shaded boxes list optimized values and the other boxes list results due to optimization.



(a) 14 selected specimens (Ave. 0.98, STD 0.17)



(b) 10 remaining specimens (Ave. 1.84, STD 0.99)

Figure 4: Comparisons between experimental and computed ultimate drifts points ( $l_p = 0.33l_w$  and  $\varepsilon_m = 2\%$ )

#### 4 CONCLUSIONS

Twenty-four reinforced concrete wall specimens were studied to simulate the ultimate drift capacity. A simple fiber based analysis combined with Beyer's shear drift model is able to provide load and drift of ultimate points by choosing a proper set of equivalent plastic hinge length ( $l_p$ ) and the limit strain of confined concrete ( $\varepsilon_m$ ). This study shows that  $l_p = 0.33l_w$  and  $\varepsilon_m = 2\%$  gave the best simulation for the ultimate drift capacity and ultimate load capacity for 14 selected specimens. However, other combinations of  $l_p$  and  $\varepsilon_m$  provide similarly good ultimate drift capacity with similar errors and the best combination of  $l_p$  and  $\varepsilon_m$  should be chosen by looking at other test results such as yielding of longitudinal bars and concrete damage.

## 5 ACKNOWLEDGEMENTS

The research was funded by the promotion of building standard provisions by the Ministry of Land, Infrastructure, Transportation and Tourism in 2011 and 2012. The project was run together with Dr. H. Fukuyama, Dr. T. Mukai, Dr. M. Tani, Prof. T. Kabeyasawa, Prof. T. Ichinose and Prof. Y. Sanada. The efforts of graduate students (Mr. K. Sakamoto, Mr. K. Toya and Mr. T. Ogura) who contributed the project are also highly appreciated.

## 6 REFERENCES

- Aaleti, S., Dai, H. and Sritharan, S. (2014). "Ductile design of slender reinforced concrete structural walls." *Proceedings of the 10th National Conference in Earthquake Engineering*, Earthquake Engineering Research Institute, Anchorage, AK.
- Architectural Institute of Japan (2012). "Reconnaissance Report on The 2010 Chile Off Maule Earthquake and Reconnaissance Report on The 2011 New Zealand Christchurch Earthquake," Arch. Inst. of Japan , p. 313.
- Beyer, K., Dazio, A. and Priestley, M.J.N. (2011). "Shear Deformations of Slender Reinforced Concrete Walls under Seismic Loading." *ACI Structural Journal*, V. 108, No. 2, pp. 167-177, 2011.
- Bohl, A. and Adebare, P. (2011). "Plastic hinge lengths in high-rise concrete shear walls." *ACI Structural Journal*, Vol. 108, No. 2, pp. 148-157.
- Dodd, L. L. and Restrepo, J. I. (1995). "Model for Predicting Cyclic Behavior of Reinforcing Steel." *Journal of Structural Engineering*, ASCE, 121(3), 433-445.
- Kabeyasawa, T., Kim, Y., Sato, M., Hyunseong, H. and Hosokawa, Y. (2011). "Tests and analysis on flexural deformability of reinforced concrete columns with wing walls." *Proceedings of the Ninth Pacific Conf. on Earthquake Eng. Building an Earthquake-Resilient Society* 14-16, New Zealand, PaperID 102.
- Kabeyasawa, T. et al. (2014). "Effects of bi-directional lateral loading on the strength and deformability of reinforced concrete walls with/without boundary columns." *Tenth National Conference on Earthquake Engineering*, July 21-25, Anchorage, USA, ID #143.
- Kono S., Tani M., Mukai T., Fukuyama H., Taleb R., Sakashita M. (2014). "Seismic behavior of Reinforced Concrete Walls for a performance based design." *Second European Conference on Earthquake Engineering and Seismology*, Aug 25-29, Istanbul, Turkey, ID #1471.
- Kowalski, M. J. (2001). "RC structural walls designed according to UBC and displacement-based methods." *ASCE Structural Journal*, Vol. 127, No. 5, pp. 506-516.
- Mander, J. B., Priestley, M. J. N., and Park, R. (1988). "Observed Stress-Strain Behavior of Confined Concrete." *Journal of Structural Engineering*, ASCE, Vol.114, No.8, August 1988, pp. 1827-1849.
- Martinelli, L. (2008). "Modeling Shear-Flexure Interaction in Reinforced Concrete, Elements Subjected to Cyclic Lateral Loading." *ACI Structural Journal*, V. 105, No. 6, pp. 675-684.
- Mostafaei, H. and Kabeyasawa, T. (2007). "Axial-Shear-Flexure Interaction Approach for Reinforced Concrete Columns." *ACI Structural Journal*, V. 104, No. 2, pp. 218 – 226.
- Ogura, T. and TANI, M. et al. (2014). "Experimental Study on Residual Damage of Full-scale R/C Nonstructural Wall Specimens." *AIJ Transactions of the Architectural Institute of Japan*, C2, pp. 447-450. (In Japanese)
- Panagiorakos, T. B. and Fardis, M. N. (2001). "Deformations of reinforced concrete members at yielding and ultimate." *ACI Structural Journal*, Vol. 98, No. 2, pp. 135-148.
- Paulay, T. and Priestley, M. J. N. (1992). "Seismic design of reinforced concrete and masonry buildings." New York, John Wiley and Sons Inc.
- Popovics, S. (1973). "A numerical approach to the complete stress-strain curve of concrete." *Cement Concrete Research*, No. 3, pp. 583-599.
- Priestley, M. J. N., Seible, F., and Calvi, G. M. (1996). "Seismic design and retrofit of bridges." John Wiley and Sons Inc., New York.
- Pugh, J.S., Lowes, L.N., Lehman, D.E. (2014). "Seismic Design of Slender Concrete Walls." *Proceedings of the 10th National Conference in Earthquake Engineering*, Earthquake Eng. Research Institute, Anchorage, AK.
- Sakino, K. and Sun, Y., (1994). "Stress-strain curve of concrete confined by rectilinear hoop." *J. Structural and Construction Engineering*, Architectural Institute of Japan, No. 461, pp. 95-104. (In Japanese)

- Takahashi, S., Yoshida, K., Ichinose, T., Sanada, Y., Matsumoto, K., Fukuyama, H., Suwada, H. (2013). "Flexural Drift Capacity of Reinforced Concrete Wall with Limited Confinement." *ACI Structural Journal*, Vol.110, No.1, pp.95-104.
- Thomsen IV, J. H. and Wallace W. J. (2004). "Displacement-based design of slender reinforced concrete structural walls – experimental verification." *Journal of Structural Engineering*, Vol. 130, No. 4, ASCE.
- Wallace, J. W. and Moehle, J.P. (1992). "Ductility and Detailing Requirements of Bearing Wall Buildings." *J. Struct. Eng.*, 118(6), pp. 1625–1644.